REAL-TIME ELECTRONIC NEURAL NETWORKS FOR ITER-LIKE MULTIPARAMETER EQUILIBRIUM RECONSTRUCTION AND CONTROL IN COMPASS-D

INSTRUMENTATION, CONTROL, AND DATA HANDLING

KEYWORDS: *neural network, plasma control, COMPASS-D*

COLIN GEORGE WINDSOR,* THOMAS NOEL TODD,
DAVID LEONARD TROTMAN, and
MICHAEL EDWARD UNDERHILL SMITH
United Kingdom Atomic Energy Authority, Government Division, Fusion, D3 Culham Laboratory, Abingdon, Oxon, OX14 3BD, United Kingdom
(*UKAEA/Euratom Association*)

Received August 9, 1995
Accepted for Publication August 12, 1996

The plasma position and shape on the COMPASS-D tokamak have been controlled simultaneously with a 75-kHz bandwidth, hard-wired, real-time neural network. The primary network operates with up to 48 selected magnetic inputs and has been used in the vertical position control loop to control the position of the upper edge of the plasma at the radius of a reciprocating Langmuir probe and to keep this constant during a programmed shape sequence. One of the main advantages of neural networks is their ability to combine signals from different types of diagnostics. Two coupled networks are now in use on COMPASS-D. A dedicated soft-X-ray network has been created with inputs from 16 vertical and 16 horizontal camera channels. With just four hidden units, it is able to accurately determine three output signals defining the plasma core radius, vertical position, and elongation. These signals are fed to the primary network along with selected magnetic inputs and four poloidal field coil control current inputs. The core data are expected to help characterize the equilibrium by providing information on the Shafranov shift and gradient of elongation, related to the equilibrium parameters β_p and l_i. This network, with 15 hidden units, is able to define 10 outputs capable of giving a parameterized display of the plasma boundary. This paper describes results from several networks trained on various combinations of inputs with (a) simulated inputs and output values, where the precision of the network can be tested; (b) experimental inputs and calculated output values, where operational precision can be tested; and (c) hardware networks, where real-time performance can be tested. The results confirm that the neural network method is capable of giving excellent precision in tokamak boundary reconstruction but that the necessary accuracy in the experimental inputs for this task is not easily achieved.

I. INTRODUCTION

Neural networks have become a standard part of the armory of methods available for control systems since the development of the multilayer perceptron method 10 yr ago.[1] Recent reviews have been given in Ref. 2 on control methods and in Ref. 3 on neural networks. In the case of the control of plasma shape and position within a tokamak, the problem of solving the Grad-Shafranov equation[4] to derive the plasma parameters from the diagnostic signals is too complex to perform on-line with present-generation digital processors but can be solved numerically to give an analysis of a particular experimental case. Alternatively, as in the neural network implementation used here, a series of numerical simulations, in which the predicted diagnostic signals are calculated

*E-mail: colin.windsor@ukaea.org.uk.

off-line for a series of possible plasma positions and shapes, can be used to form a training database. The neural network thus operates by performing a nonlinear mapping between the multidimensional input space of the various diagnostic variables to an output space containing the desired parameters to be measured or controlled. The method can be characterized as one of "learning by example." The operation of the method was described by Bishop et al.,[5] who implemented a real-time network on the COMPASS-D tokamak based on magnetic diagnostic inputs. Off-line analysis to derive plasma parameters had been implemented earlier by Lister and Schnurrenberger[6] and Lister et al.[7]

Neural networks are not the only method capable of learning by example from a database of representative plasma equilibria. Function parameterization represents a conventional approach to the same task. Both input and output variables are linearly combined to derive their principal components, which are then fitted using up to third-order Hermitian polynomials. The method is fast enough for on-line use. Work by Wijnands[8] suggests that function parameterization is somewhat less accurate than neural networks, working from the same database.

II. COMPASS-D AS A TEST BED FOR ITER

Although smaller than the International Thermonuclear Experimental Reactor (ITER) by a factor of ~15, the COMPASS-D tokamak at Culham Laboratory in the United Kingdom is well suited to trial studies of plasma position control. It mimics ITER in featuring a strongly asymmetric divertor configuration with a single lower-null *X* point. Unlike many larger facilities, it is small enough to allow novel control diagnostics and systems to be tested comprehensively. The plasma currents are typically of the order of 200 kA, and the q_{95} values are in the range of 2.5 to 6.0. We assume here that the parameter accuracies possible on COMPASS are relevant to ITER when scaled by the factor 15. This should be generally true for the magnetic diagnostics because they scale with the plasma current. It may be less true for the soft-X-ray (SX) signals. A problem with ITER is that its long pulses and high levels of fast neutron radiation mean that magnetic diagnostics close to the plasma may not be reliable in the long term. This study, therefore, considers the alternatives of control current (CC) inputs, remote flux loops (FLs), and SX emission.

COMPASS-D is driven by four independent poloidal field current controllers, ignoring the fast vertical controller. Although the circuits in which these currents flow can be rearranged to give various field configurations, all the simulated shots in the database used (and the real shots analyzed during this study) corresponded to an ITER-like, single-null divertor configuration. It is therefore valid to consider the use of CCs as diagnostic inputs.

Although COMPASS-D has several sets of magnetic diagnostics, the present study considers only 5 FLs installed close to the plasma, 5 remote FLs at a distance from the plasma roughly corresponding to the ITER outer blanket wall, and 22 saddle loops (SAs) on the vacuum vessel arranged in summed pairs from opposite quadrants of the torus. The remote loops are placed around the outer mechanical structure of COMPASS-D. The simulations use flux difference measurements, where that from the near-midplane signal (coil number 3) is subtracted from all other signals, to give just four difference signals. Figure 1 shows the positions of these coils in the poloidal cross section compared with the COMPASS-D vessel and CC coils.

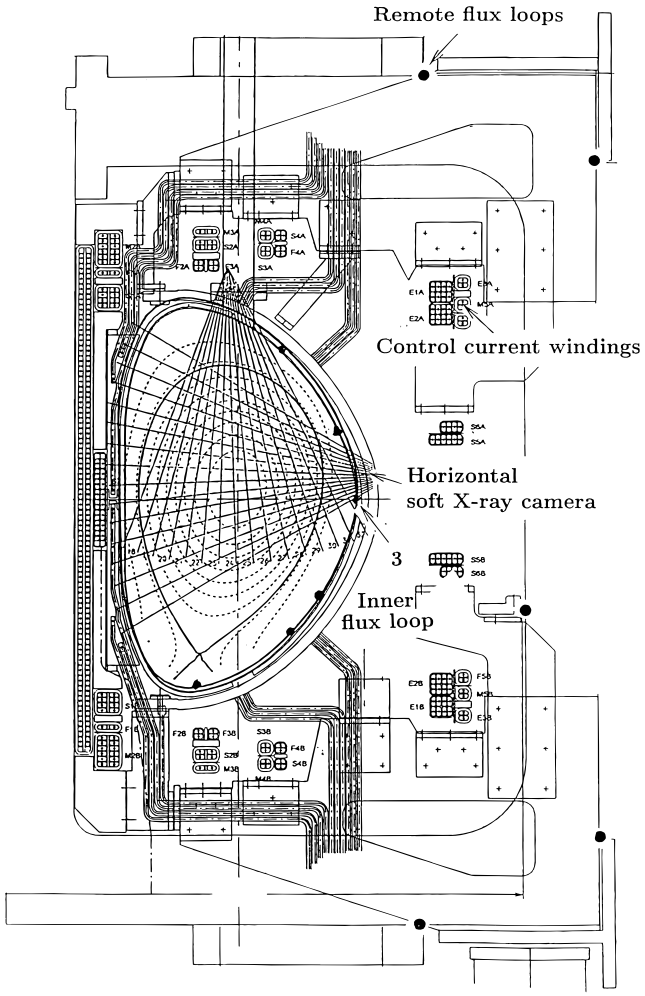

Fig. 1. The poloidal cross section of the COMPASS-D tokamak at Culham showing the vessel boundary and structure and a typical plasma with lower *X* point. The CC windings are shown by the arrays of small squares, the positions of the inner and outer FLs are shown by the black circles with arrows, and the chordal views from the individual channels of the horizontal and vertical SX cameras are shown by the full lines.

The other COMPASS diagnostics considered here are the horizontal and vertical SX cameras. The 16 views across the plasma given by each of the two cameras are shown by the radiating lines in Fig. 1. X-ray emission rises sharply with the plasma density and temperature and so is most sensitive to the conditions in the center of the plasma where these are highest. Absolute calibration of the X-ray emission is complicated by the spectral sensitivity and by the effects of impurities. However, the relative distribution of the X-ray emission intensity across the camera field of view, simulated in Fig. 2 for a typical *X*-point plasma, gives the radius and vertical position of the core of the plasma. The ratio of the vertical and horizontal widths of the X-ray emission gives a good measure of the core elongation, independently of the exact functional form of the emission, as long as the contours of the X-ray emission follow the poloidal flux surfaces.

III. THE OPERATION OF NEURAL NETWORKS

The 5 inner FLs and 22 SAs were first used in April 1994 as inputs for the hardware neural network used to control such parameters as the position of the top of the plasma surface at the radius of the reciprocating Langmuir probe. Figure 3 shows an example of both position and shape control of the plasma. In this shot, a network with just two output variables was used to stabilize the vertical position of the plasma at the radius of the reciprocating probe, while the elongation was feedback controlled to track a prescribed variation. Both parameters were trained with offsets (1 in κ and 0.05 m in Z_{probe}), so that the output range of the neural network lay in the 0- to 5-V range, where the hardware has optimal performance. The network elongation output follows closely the programmed variation, although the magnitude is a little less due to loop gain effects.

Here, neural networks are used to evaluate the accuracy in selected plasma parameters that might be achievable from various possible combinations of diagnostic inputs. A neural network may be set up so that its outputs provide a direct measure of those parameters that need to be precisely controlled. For example, on ITER, four gaps between the plasma boundary and the limiter, together with the positions of the plasma strike points on the diverter target, might be chosen.[9] For the present study, a set of 10 parameters that are convenient for a parameterized description of the plasma boundary and profile has been defined. These are the plasma inner radius R_p, vertical position Z_p, minor radius a, elongation κ, triangularity δ, X-point radius R_x, vertical position Z_x, core radius R_c, vertical position Z_c, and elongation κ_c. The present

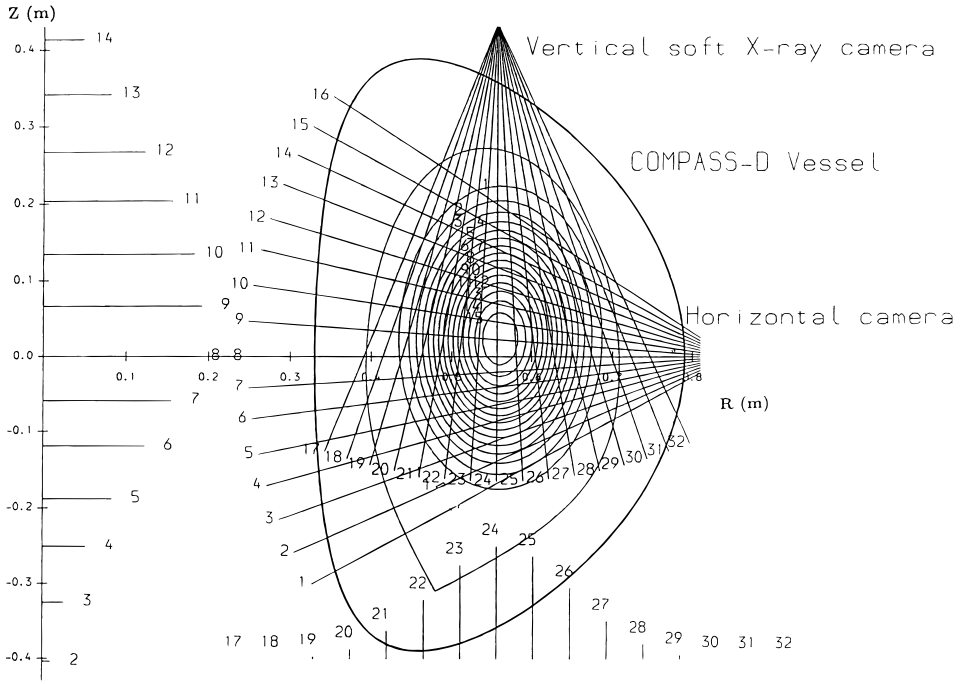

Fig. 2. The chordal SX intensities from the simulated plasma equilibrium shown. The vessel is shown by the heavy line. The plasma boundary is shown as described in Sec. III by the plasma inner radius R_p, vertical position Z_p, minor radius a, elongation κ, triangularity δ, X-point radius R_x, and vertical position Z_x. The pressure contours are centered on the core radius R_c and vertical position Z_c, with core elongation κ_c. The intensity histograms at the left and bottom of the figure show the chordally integrated SX intensity for each of the corresponding channels.

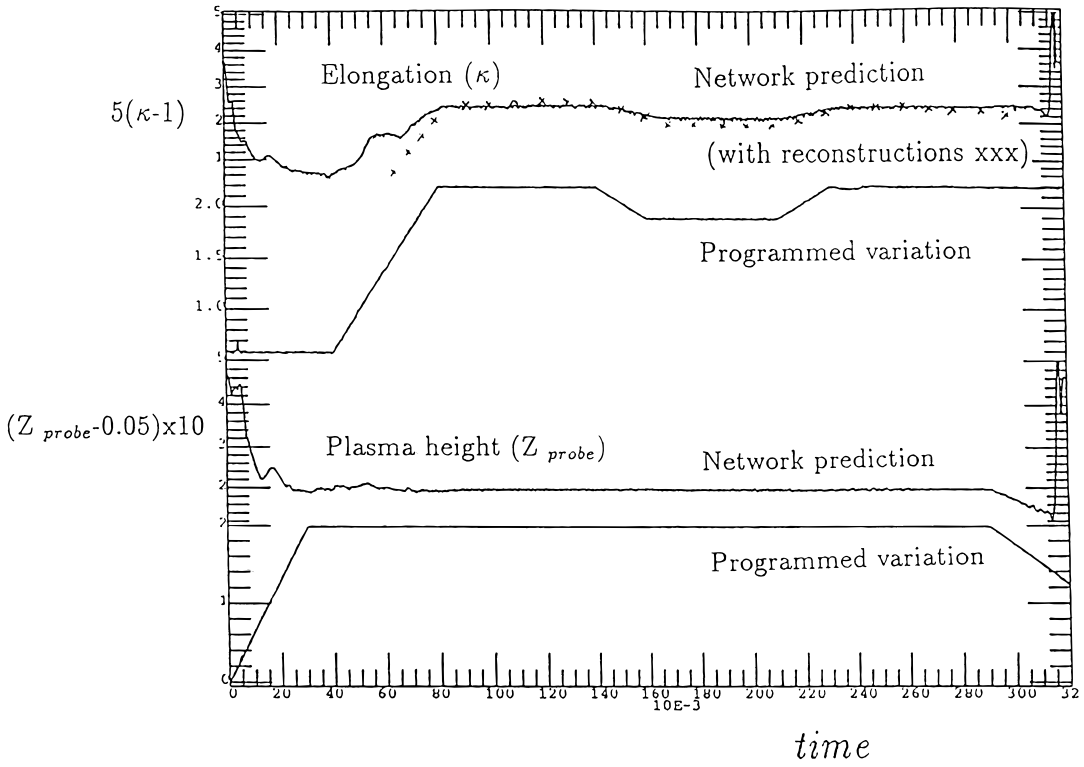

Fig. 3. The control of both plasma shape and top surface position of COMPASS-D for shot 13804. The upper traces show the elongation given by the network compared with the programmed variation as a function of the time in seconds. The lower traces show the corresponding values for the vertical position of the plasma upper boundary at the radius of the reciprocating probe. The crosses represent the output of a filament code (DFIT) matched to the measured data.

parameterization of the plasma boundary uses, for circular plasmas and the upper section of *X*-point plasmas, the positional variation as a function of poloidal angle θ given by

$$R(\theta) = R_p + a\cos(\theta + \delta\sin\theta) \ ;$$
$$Z(\theta) = Z_p + a\kappa\sin\theta \ . \qquad (1)$$

The lower section of an *X*-point plasma is defined by an approximate polynomial function

$$(R - R_p \pm a) = \pm[A2(Z - Z_p)^2 + A4(Z - Z_p)^4 + A6(Z - Z_p)^6] \ , \qquad (2)$$

where the coefficients *A*2, *A*4, and *A*6 are evaluated so that the boundary goes through the desired R_x, Z_x and through the midplane with the curvature calculated from Eq. (4); i.e.,

$$A2 = \frac{C}{2} \ ; \qquad A4 = \frac{(30R_x - 14CZ_x^2)}{18Z_x^4} \ ;$$
$$A6 = \frac{(-12R_x + 5CZ_x^2)}{18Z_x^6} \ , \qquad (3)$$

where the curvature C at R_0, Z_0 is given by

$$C = \frac{(1 \pm \delta)}{a\kappa^2} \ . \qquad (4)$$

This parameterization has the advantage of needing only 6 parameters and gives a reasonable description of an *X*-point boundary, as shown in Fig. 2. It has the defect of showing a slightly unphysical vertical boundary at the plasma midplane. The SX emission E was evaluated by integration along the viewing chords through the plasma with a parameterized pressure dependence, enhanced by a power law variation of the form $E = p^n$, where the exponent n is at present set equal to 2, representing approximately the convolution of bremsstrahlung radiation and the detector behavior. The ITER neutron emission profile would similarly be a function of temperature and density.

Figure 4 shows the parameterized plasma boundaries for the 501 simulated shots in the database used. The database contains both predicted diagnostic values and plasma boundary parameters for each shape shown. One sees that it covers a wide range of plasma shapes and positions. Network training consists of continually presenting the training fraction of these simulated shots to the network and

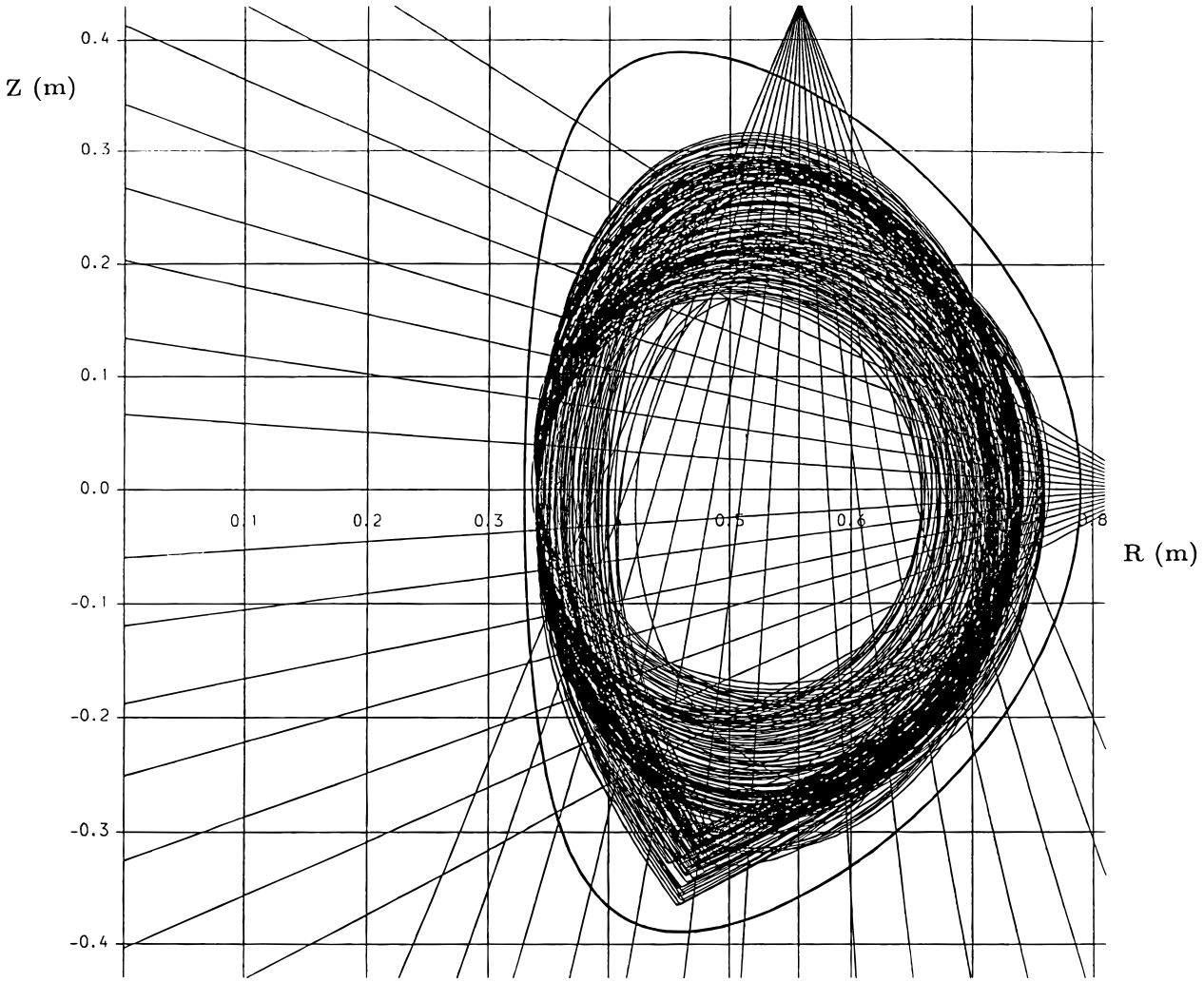

Fig. 4. The plasma boundaries for the 502 simulated shots in the database expressed through the 7 parameters: R_p, Z_p, a, κ, δ, R_x, and Z_x.

adjusting the ~400 weights until the output parameters describing the plasma shape are as close as possible to their targets. The actual number of weights used depends on the number of inputs n_i, the number of hidden units n_h, and the number of outputs n_o. Including the threshold weights, it is given by $n_i(n_h + 1) + n_h(n_o + 1)$ and varies from 133 for the smallest networks to 457 for the largest.

Networks considered for this study include the single networks as follows:

case 1. 5 inner FLs only (5 FL)

case 2. 4 CCs only (4 CC)

case 3. 32 SX inputs only (32 SX)

case 4. 5 inner FLs and 4 CCs only (5 FL + 4 CC)

case 5. 5 inner FLs and 21 SAs only (5 FL + 21 SA)

case 6. 5 inner FLs and 32 SX inputs only (5 FL + 32 SX)

case 7. 5 inner FLs, 32 SX inputs, and 4 CCs (5 FL + 32 SX + 4 CC).

Also considered are the following double networks, where the first network consists of 32 SXs, giving 3 SX outputs (SXOs) (3 SXO), R_c, Z_c, and κ_c, which are fed to the second network. The advantage of the double network is that in its hardware implementation, the training and testing of the SX network may be completely separated from that of the main network:

case 8. R_c, Z_c, κ_c, and 5 FLs only (3 SXO + 5 FL)

case 9. R_c, Z_c, κ_c, and 4 CCs only (3 SXO + 4 CC)

case 10. R_c, Z_c, κ_c, 4 CCs, and 5 inner FLs (3 SXO + 5 FL + 4 CC).

For all the options, it is possible to estimate the theoretical accuracy achievable by the neural network for equilibria represented in the training database, which for this purpose is divided into equal populations of training and testing shots. The results from this case are considered in Sec. IV for diagnostic inputs that are varied by a nominal Gaussian distribution with a standard deviation of 2% to allow for experimental uncertainties. However, they cannot be trusted to represent the true experimental situation, where systematic experimental errors from alignment uncertainties, integrator drift, incorrect SX modeling, and various irradiation effects in ITER must be included.

The results described in Sec. V will include such effects in the case of COMPASS-D by using diagnostic inputs from actual shots. In this case, the true boundary parameters are not known and must be estimated from, for example, putting a full set of close-in magnetic diagnostic inputs into a filament inversion code and comparing the results with the boundary parameters predicted by the network. Clearly, such a process compounds any error due to the neural net prediction with the error from the filament code inversion process itself. The process is not yet possible with networks involving the outer FLs. The results of Sec. V will be presented for simulated networks, which have been shown to mirror very closely the actual hardware networks installed on COMPASS-D.

IV. THEORETICAL PLASMA BOUNDARY ACCURACY EVALUATED FROM THE DATABASE

This section evaluates the mean accuracy of the plasma boundary parameters (in millimetres) for COMPASS-D for the various networks. Values scaled by a factor 15 to correspond to the ITER case are also given. The input data for each diagnostic have had a variable

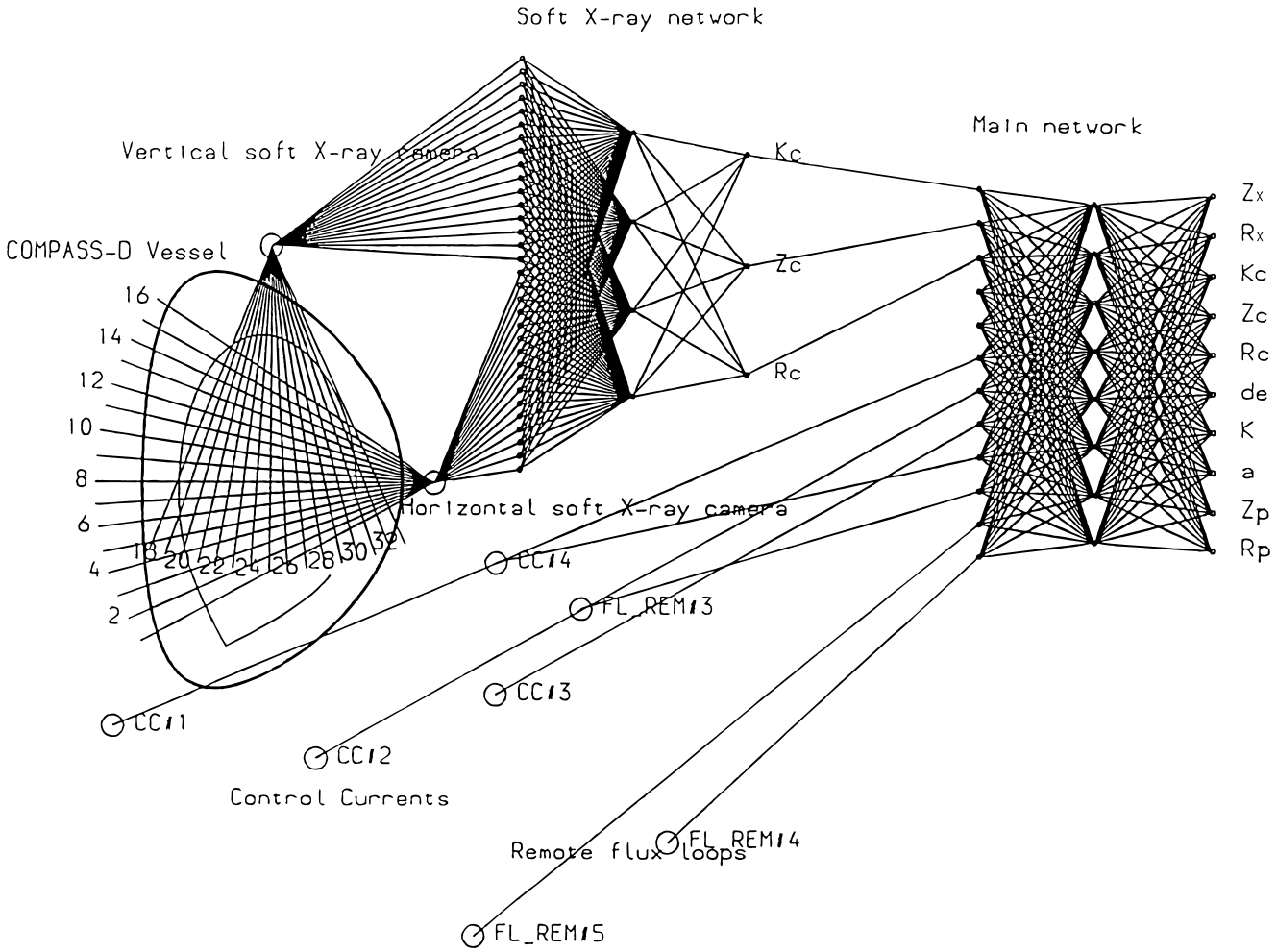

Fig. 5. A schematic diagram of the double neural network as simulated and installed on COMPASS-D. The two SX cameras define 32 inputs to a dedicated SX network. Its outputs are fed, together with remote magnetic FL and CC data, to the main network, which evaluates the 10 plasma parameters shown.

percentage of random Gaussian noise added to simulate experimental errors. In the first instance, 0 or 2% was added; however, for some cases, the spread in the SX values was increased to 10% with a minimum spread of ~10% of the peak intensity. The networks were trained for at least 10 000 iterations, which previous studies with this database have shown to give adequate convergence.[10] The 251 training examples in the database were presented to the network, and the performance quoted here refers to the absolute error between the network predictions and the true values for the 250 test examples in the database.

An important parameter is the number of hidden units in the network. Several tests[10] have been made in which the test performance is plotted against the number of hidden units. Generally, there is a shallow minimum at ~8 to 16 hidden units for this type of problem, and values in this range have been chosen in this study.

The estimate of the accuracy of the prediction of the main boundary may be defined in units of millimetres from the average accuracy achieved in the parameters R_p, Z_p, a, and the product $a\kappa$. The X-point position is usually less well characterized and will be separately defined by the average accuracy of R_x and Z_x. The accuracy of the three core parameters is defined from the average accuracy achieved in the three lengths R_c, Z_c, and the product $a\kappa_c$. These three averages will be used to define the accuracy of the neural network predictions.

Table I confirms many intuitive concepts. The 5 FLs alone, listed as case 1 in Table I, give a fair performance with an error of the order of 5 mm in the boundary and core dimensions and a larger (15-mm) error in the X-point position. The 4 CCs alone (case 2) give 50% larger errors but when included together with the FLs (case 4) give significantly smaller errors. The 32 SX channels alone (case 3) give poor boundary accuracy and very poor X-point accuracy but excellent accuracy in the core dimensions, that is, a factor of 4 better than with the 5 FLs alone. This accuracy is only reduced by 50% when the simulated noise in the peak channel is increased by a factor of 5, and that in the wings is increased by an even larger factor.

The good performance in the core parameters provides the rationale for the double networks, as illustrated in Fig. 5. The first network analyzes only the SXs and has just three output parameters defining the core radius, vertical position, and elongation. The outputs of this first network are fed along with other diagnostic inputs to the main network defining the plasma boundary. The 10 outputs of the main network give the parameters R_p, Z_p, a, κ, δ, R_c, Z_c, κ_c, R_x, and Z_x, defined in Sec. III. These parameters are correlated in that, for example, the Shafranov shift, the

TABLE I

The Accuracy in the Plasma Parameters Achieved by the Neural Network Compared with Their Database Values for Test Examples*

Case	Single Network Inputs	X-Ray Spread (%)	Hidden Units	Boundary Error (mm)	X-Point Error (mm)	Core Error (mm)	Scaled Boundary (mm)	Scaled X Point (mm)	Scaled Core (mm)
1	5 FLs	0	8	4.1	16.5	5.3	61.6	248.0	78.9
	5 FLs	2	8	4.0	17.2	5.4	60.0	258.6	80.6
2	4 CCs	2	12	6.1	19.8	7.0	91.1	296.3	105.8
3	32 SXs	2	8	5.1	38.9	1.5	76.9	583.3	22.6
	32 SXs	10	8	8.4	59.3	3.9	108.6	771.4	50.3
4	5 FL + 4 CC	2	8	2.7	20.7	4.1	40.0	311.1	62.1
5	21 SA + 5 FL	8	2	2.2	17.4	3.1	33.0	261.4	46.0
6	32 SX + 5 FL	8	2	2.2	29.7	1.1	33.6	445.2	15.9
7	32 SX + 5 FL + 4 CC	0	8	2.4	19.7	2.3	36.5	295.7	34.1
	32 SX + 5 FL + 4 CC	2	8	1.9	23.9	0.7	28.5	358.5	10.5
	32 SX + 5 FL + 4 CC	10	8	3.8	31.6	4.7	57.0	474.2	70.3
	Double Network Inputs								
8	3 SXO + 5 FL	2	4 + 8	3.4	33.4	2.8	51.4	501.2	42.5
9	3 SXO + 4 CC	2	4 + 6	4.0	20.4	2.7	59.3	306.8	39.8
10	3 SXO + 5 FL + 4 CC	2	4 + 8	2.3	22.6	2.1	34.7	338.8	31.2

*The boundary error corresponds to the mean error in 4 boundary length parameters, the X-point error to that of the 2 X-point coordinates, and the core error to the 3 core length parameters, as defined in Sec. IV. The scaled values are multiplied by 15 to correspond to the case of ITER.

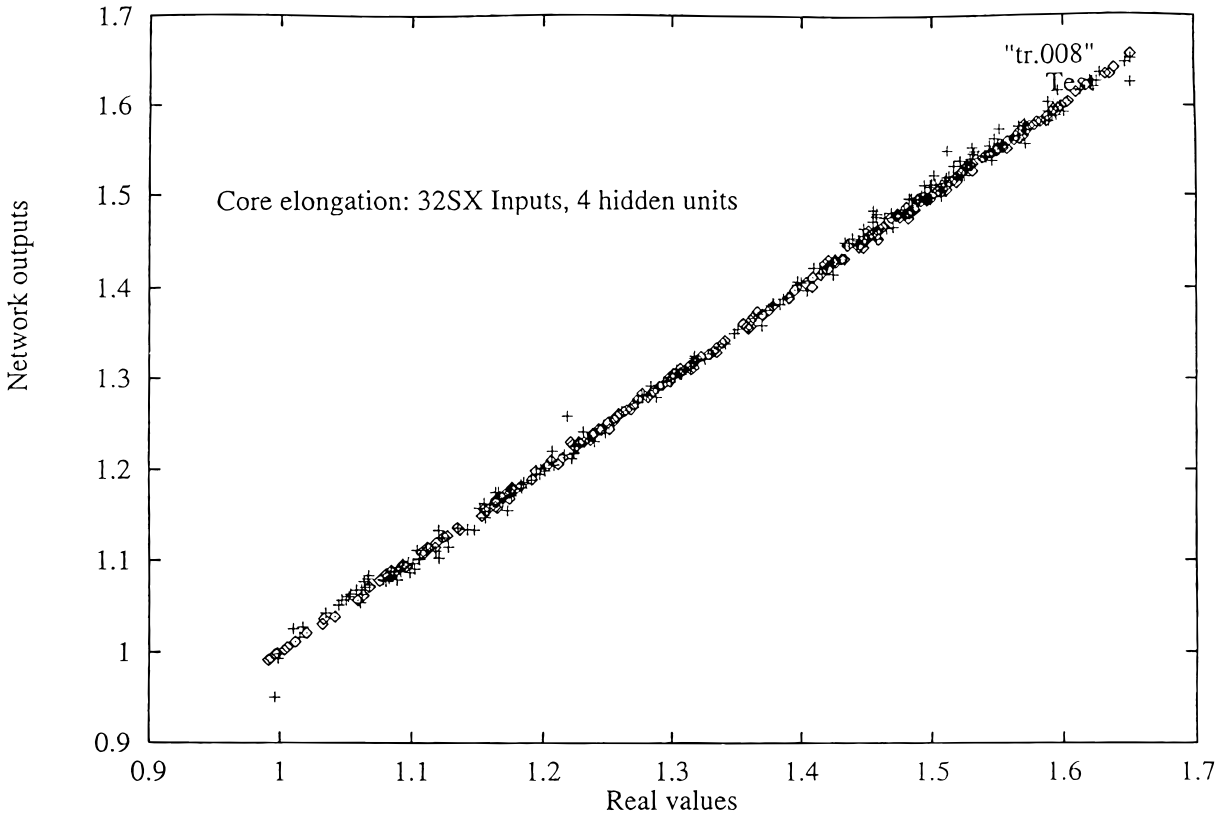

Fig. 6. A comparison of the core elongation given by the output of the SX network, compared with its actual value. The crosses denote the testing examples, and the diamonds denote the training examples.

difference between the plasma magnetic and core radii, is related to the aspect ratio and elongation. However, the hidden units of a neural network are able to use such correlations to maximum advantage.

Figure 6 shows an example of the very good simulation performance of this primary network for the case of core elongation. The crosses show for test data the elongation predicted by the network compared with the actual value. This network has an overall performance, as shown in Table II, of ~3-mm accuracy in the core position and 0.01-mm accuracy in the core elongation.

There is evidently some cost in this procedure because a double network fed by 32 SX channels and 5 FLs (case 8) has a significantly worse performance overall than the single network with the same inputs (case 6). This is also seen in the comparison of networks for cases

TABLE II

Test Error in the Core Positions and Elongation for the 3-Output SX Network with the 32 SX Inputs Only*

Case	Spread (%)	Hidden Units	Radius Error (mm)	Position Error (mm)	Core Elongation	Scaled Radius (mm)	Scaled Position (mm)
1	2	4	3.5	3.9	0.0098	52.5	58.5
2	2	8	3.1	4.1	0.0095	46.5	61.5
1	10	4	1.8	1.8	0.045	27.8	27.0
2	10	8	1.5	1.5	0.045	22.5	22.5
3	10	16	1.5	1.4	0.049	22.5	21.0

*The scaled values are multiplied by 15 to correspond to the case of ITER.

7 and 10. Part of this deterioration is the further 2% error that was added to the SX network outputs to allow for possible errors introduced by the network itself. The double network still performs appreciably better than that with FL inputs alone, especially in the plasma core parameters. Double networks with SXOs included with CCs (case 9) and with both FLs and CCs (case 10) provide steadily improved performance as more diagnostic inputs are added, with the networks including SXOs, FLs, and CCs having the best overall performance of all the networks considered.

V. THE PLASMA BOUNDARY ACCURACY ACHIEVED FROM EXPERIMENT

This section considers the boundary accuracy achieved for particular shots on COMPASS-D using various combinations of diagnostic inputs to the neural network. Experimental errors caused by integrator drift, calibration errors, and noise are now necessarily included. In the case of SXs, there is a possible leakage current, providing a variable background to the signal. There is a problem with the analysis of the results in that

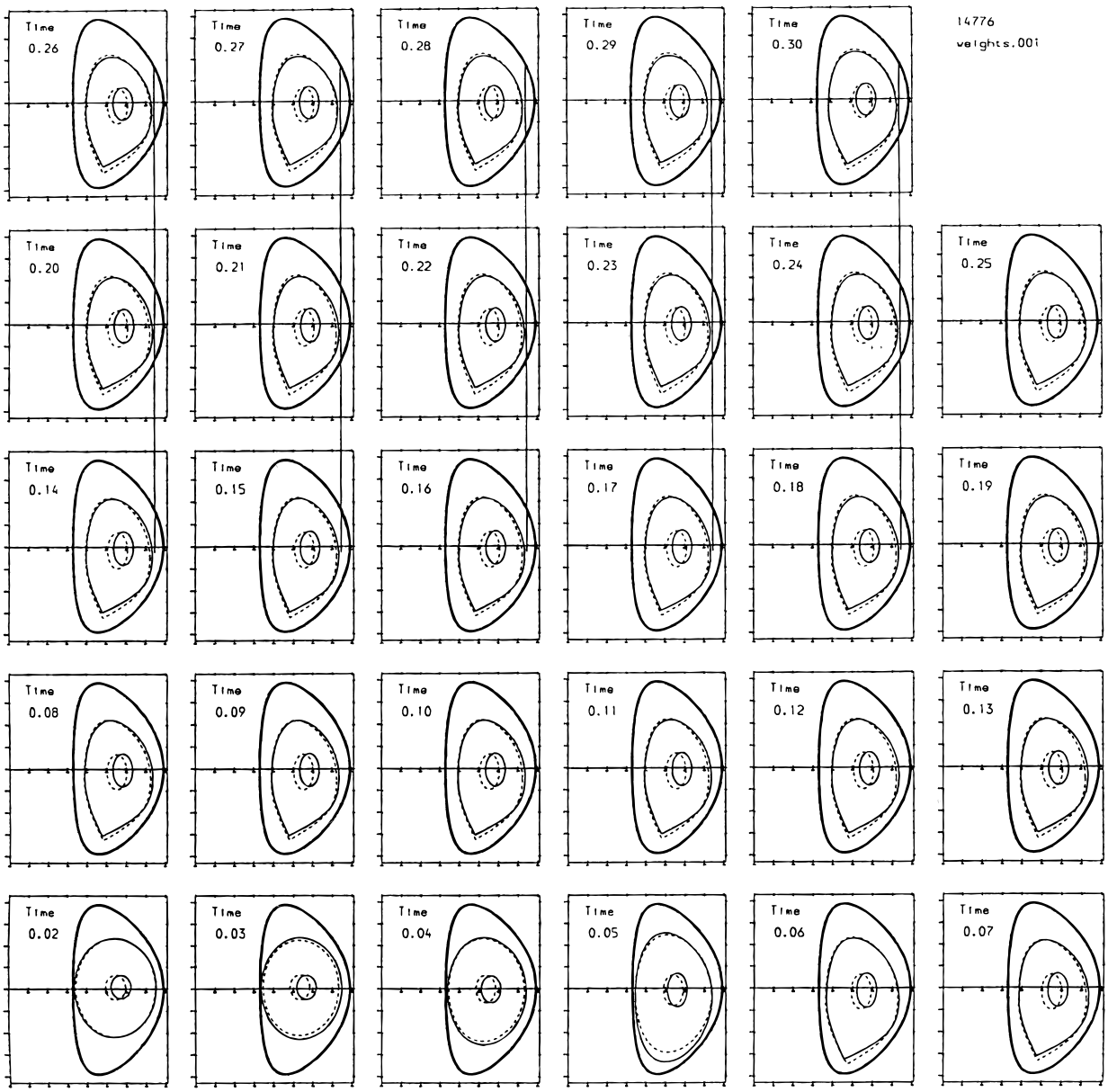

Fig. 7a. Accuracy of predictions for case 1 with 5 close-in FLs only.

the true answer is no longer at hand and must be evaluated approximately from some numerical code with its own attendant errors. In this case, it has been evaluated from the DFIT filament code.[11] Each shot gives a time series of different configurations that all may be used to test the reconstruction accuracy. For the present analysis, each shot has been divided into 29 time slices at 0.01-s intervals, from 0.02 to 0.30 s.

The input variables are read in from the COMPASS database of files. The data are stored at intervals of 150 μs, and the data at each start time have been averaged over 0.005 s to remove any fluctuations that may exist over shorter timescales. Magnetic signals are generally proportional to the plasma current, so that the training database has been generated for a fixed plasma current of 400 kA, and the network magnetic inputs have been normalized to this according to the measured instantaneous value of the current. Other diagnostic inputs are treated differently. The signals from the two SX cameras, for example, are each separately normalized to the signals of their central channel.

The results in this section have been obtained from simulations of the neural networks rather than from real-time hardware networks. However, our previous studies

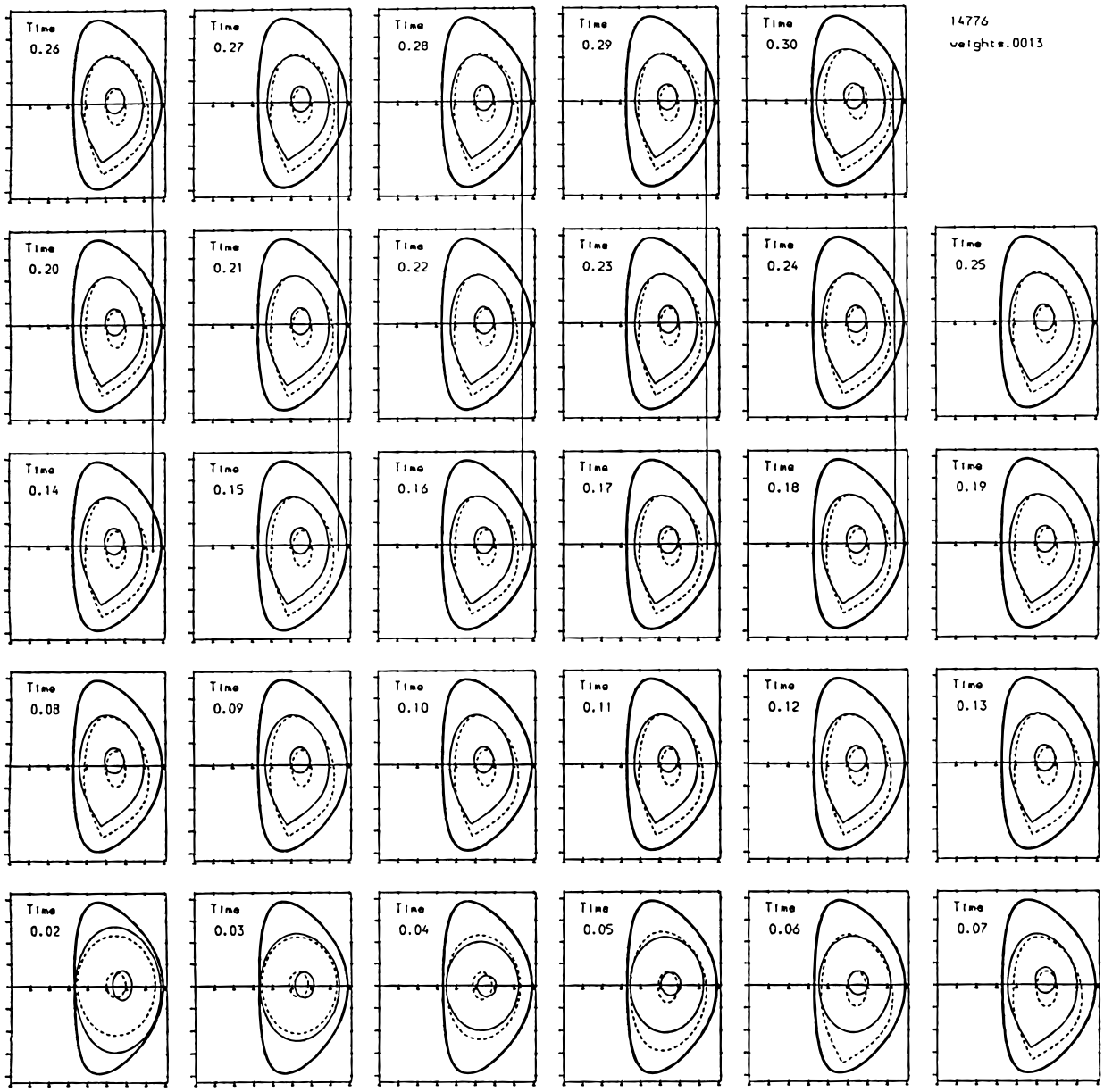

Fig. 7b. Accuracy of predictions for case 9 with a double network merging SX and CC inputs only.

show that these simulations agree closely with the actual outputs of hardware networks.[10] The simulated networks are used to predict the plasma boundary, as defined in Sec. III by 10 output parameters. As in Sec. IV, the results are given both for single networks and for double networks where the first analyzes just the SX data to give outputs describing the core parameters, which are then fed as inputs to the second network. The accuracy of the predictions may be judged by Fig. 7. These show by the full lines, for various sets of experimental inputs from shot 14776, the plasma boundary predicted by the neural network simulator and, near the center of the plasma, the boundary of the core region at a fixed minor radius of 50 mm. The inner lines show the predicted plasma core position and elongation at one-third of the minor radius. The dashed lines show the boundaries given using the corresponding parameters predicted by the DFIT filament code from extensive magnetic data including both FLs and external partial Rogowski coils. The degree of agreement between the two boundaries indicates the corresponding agreement between the 10 parameters used to define these approximate boundaries, as calculated

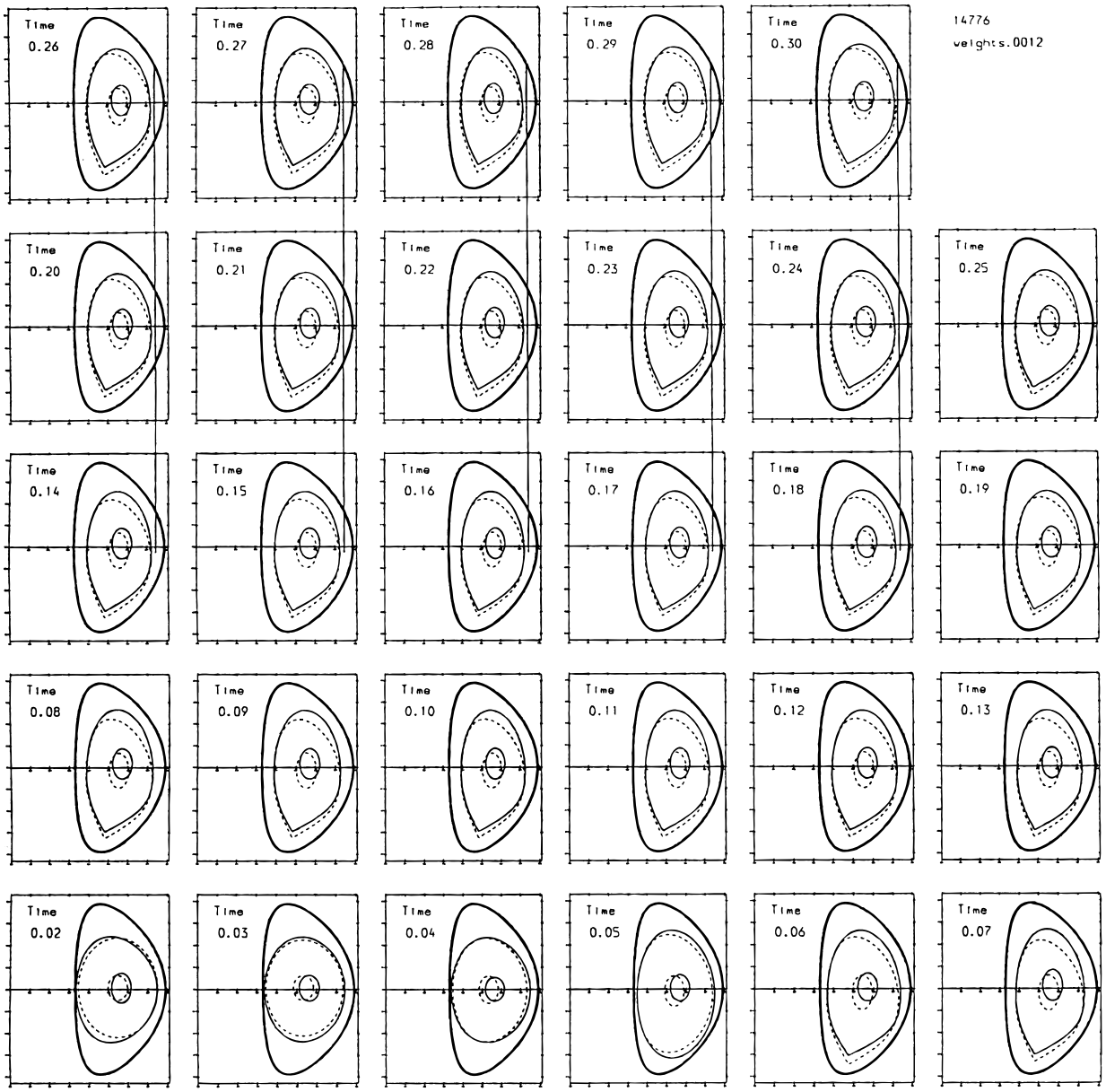

Fig. 7c. Accuracy of predictions for case 10 with a double network using the 32 SX inputs in the first network and its outputs together with magnetic and CC signals in the second.

using the neural net and as found from DFIT. Because filament codes cannot calculate an independent core position or elongation with any precision, the core accuracy results can be only illustrative.

Figure 7a is for the 5 FLs alone (case 1) and gives a fair picture of the evolution of the shot. In particular, the initial elongation increase is well described. The core position given by the network is consistently outside the DFIT prediction, but this may well be an artifact of a filament code based on magnetic data alone. Figure 7b is for a double network with SXs and CCs only, with all torus-based magnetic information (case 9) omitted. The *X*-point is rather poorly judged, but the reconstruction is otherwise quite good. Figure 7c is the double network with SX, CC, and magnetic inputs (case 10). The data may also be expressed as a time-dependent moving image as in Fig. 8, which corresponds to case 1 given in Fig. 7a.

All sets of data are analyzed in Table III to give a quantitative estimate of the error in the plasma parameters. The boundary error is the average over the differences in the four length parameters R_p, Z_p, a, and $a\kappa$ between the network predictions and those of DFIT. The *X*-point error is the corresponding average error in the two length parameters R_x and Z_x. The core error is that for the three length parameters R_c, Z_c, and $a\kappa_c$. The *X*-point averages are taken only over the period from 0.06 to 0.30 s when the *X* point exists.

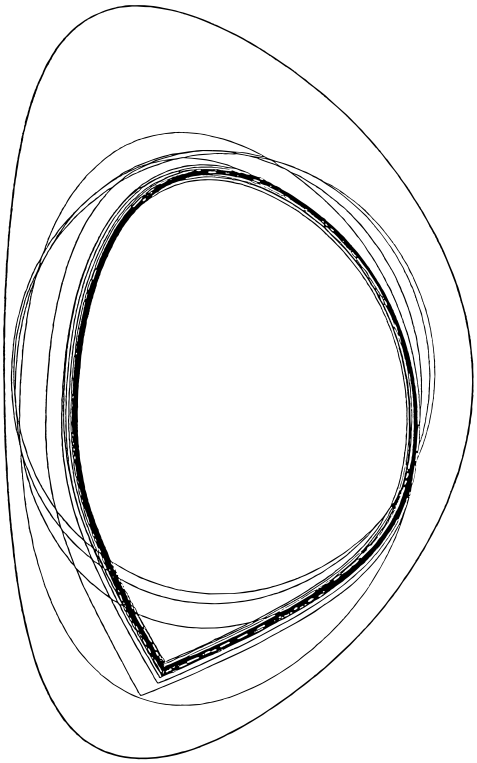

Fig. 8. The plasma boundary predicted from the network from experimental data from shot 14776. The lines show a superposition of the boundaries as a function of time. This figure corresponds to case 1 with 5 inner FLs only, as shown in Fig. 7a.

Generally, the precision of the results is very much worse than in the case of the pure simulations given in Table I. However, the results are being refined at present, and the present results must be regarded as preliminary. The neural network parameters, being based on the inversion of the Grad-Shafranov equation, are not expected to agree too closely with those from a filament code.

It is noticeable that in some cases, such as in the SX reconstructions, cases 3 and 4 in Table III, all three measures of the accuracy improve as the spread in the training X-ray signal increases. This is because the small spurious signals in the wings of the X-ray distribution, caused by leakage currents, are treated with less weight than are the larger central signals. With inappropriate training errors, the addition of extra information can give worse results, as in case 7, which adds SX inputs, compared to case 4. With optimal training errors as in case 10, the accuracy is much improved.

In particular, it is necessary to consider the accuracy achieved as a function of time through the shot. At both early and late times, the SX intensity is very low, and good results cannot be expected. Around the middle of the shot when the plasma pressure is high and the SX signals are large, much better results can be achieved. This is illustrated in Fig. 9, which shows the three accuracy parameters, as defined earlier in this section, evaluated at a given instant and expressed as a function of time.

VI. REAL-TIME SX RESULTS

Figure 10 shows early results from the real-time SX network and corresponds to the time range from 0.25 to 0.255 s, with the points plotted at spacings of 150 μs. The upper curve shows a simulation of the core elongation output of the network, while the lower curve shows the measured output from the hardware before scaling and offset subtraction. The ability of the net to respond to the rapid signals is clearly shown.

VII. CONCLUSIONS AND WORK IN PROGRESS

The results of Sec. IV, using simulations from the database, show clearly that the neural network method would be capable of determining the ITER plasma boundary to the required accuracy given that the experimental diagnostic inputs to the network were of an adequate accuracy and that the assumed size scaling is valid. They show also that SX data give much improved accuracy to the boundary prediction. The additional information they give would be more important for the long pulses of ITER.

TABLE III

The Accuracy in the Plasma Parameters Achieved by the Neural Network with Experimental Data Inputs Compared with the Corresponding Values Given by the DFIT Filament Code*

Case	Single Network Inputs	*X*-Ray Spread (%)	Hidden Units	Boundary Error (mm)	*X*-Point Error (mm)	Core Error (mm)	Scaled Boundary (mm)	Scaled *X* Point (mm)	Scaled Core (mm)
1	5 FLs	2	8	8.7	11.7	19.0	130	175	285
2	4 CCs	2	12	8.5	12.7	13.2	127	190	198
3	32 SXs	2	8	43.7	379.1	38.2	655	5686	573
3	32 SXs	10	8	43.6	347.8	39.9	654	5217	598
4	5 FL + 4 CC	2	8	36.4	117.6	57.0	546	1764	855
5	21 SA + 5 FL	2	8	33.5	19.4	51.0	502	291	765
6	32 SX + 5 FL	10	8	10.8	15.7	19.4	162	235	291
7	32 SX + 5 FL + 4 CC	2	8	55.8	33.8	89.9	837	507	1348
7	32 SX + 5 FL + 4 CC	10	8	54.2	32.1	84.1	813	483	1261
	Double Network Inputs								
7	3 SXO + 5 FL	2	4 + 8	27.4	14.3	28.6	411	214	429
7	3 SXO + 5 FL	10	4 + 8	16.3	25.2	46.9	244	378	703
8	3 SXO + 4 CC	2	4 + 8	23.5	20.5	36.8	379	307	552
8	3 SXO + 4 CC	10	4 + 8	27.5	35.2	42.3	412	528	634
10	3 SXO + 5 FL + 4 CC	2	4 + 8	24.3	11.1	35.3	364	166	529
10	3 SXO + 5 FL + 4 CC	10	4 + 8	9.7	17.0	30.2	145	255	453

*The boundary error corresponds to the mean error in 4 boundary length parameters, the *X*-point error to that of the 2 *X*-point coordinates, and the core error to the 3 core length parameters, as defined in Sec. V. The scaled values are multiplied by 15 to correspond to the case of ITER.

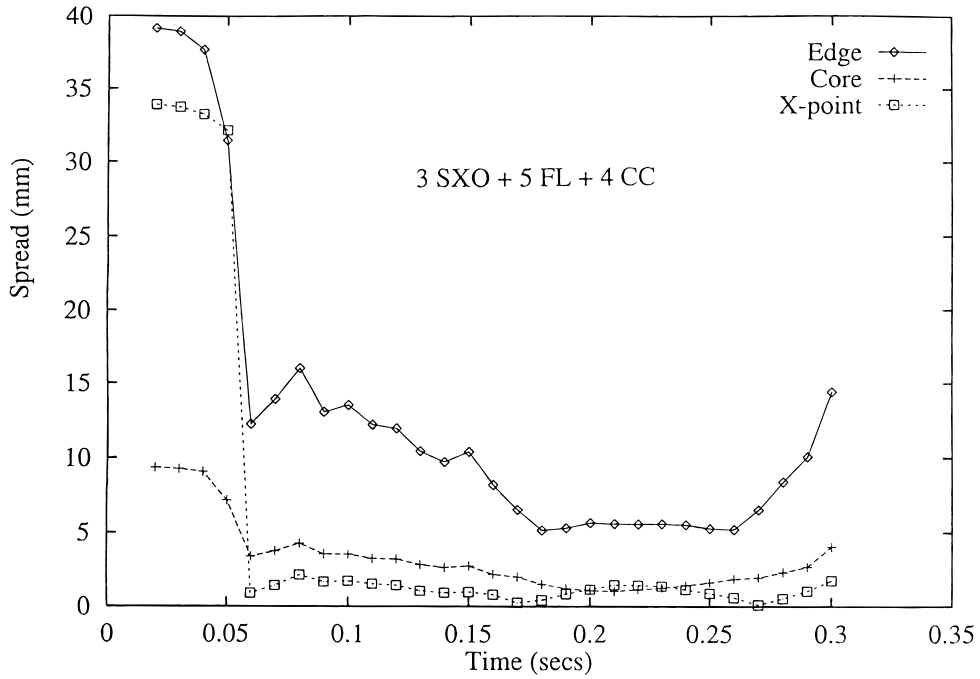

Fig. 9. The average accuracy of the parameters defining the boundary, *X*-point, and core dimensions (in millimetres) as a function of time for the double network (case 10) showing the much better performance in the middle period of the shot when the SX intensity is high.

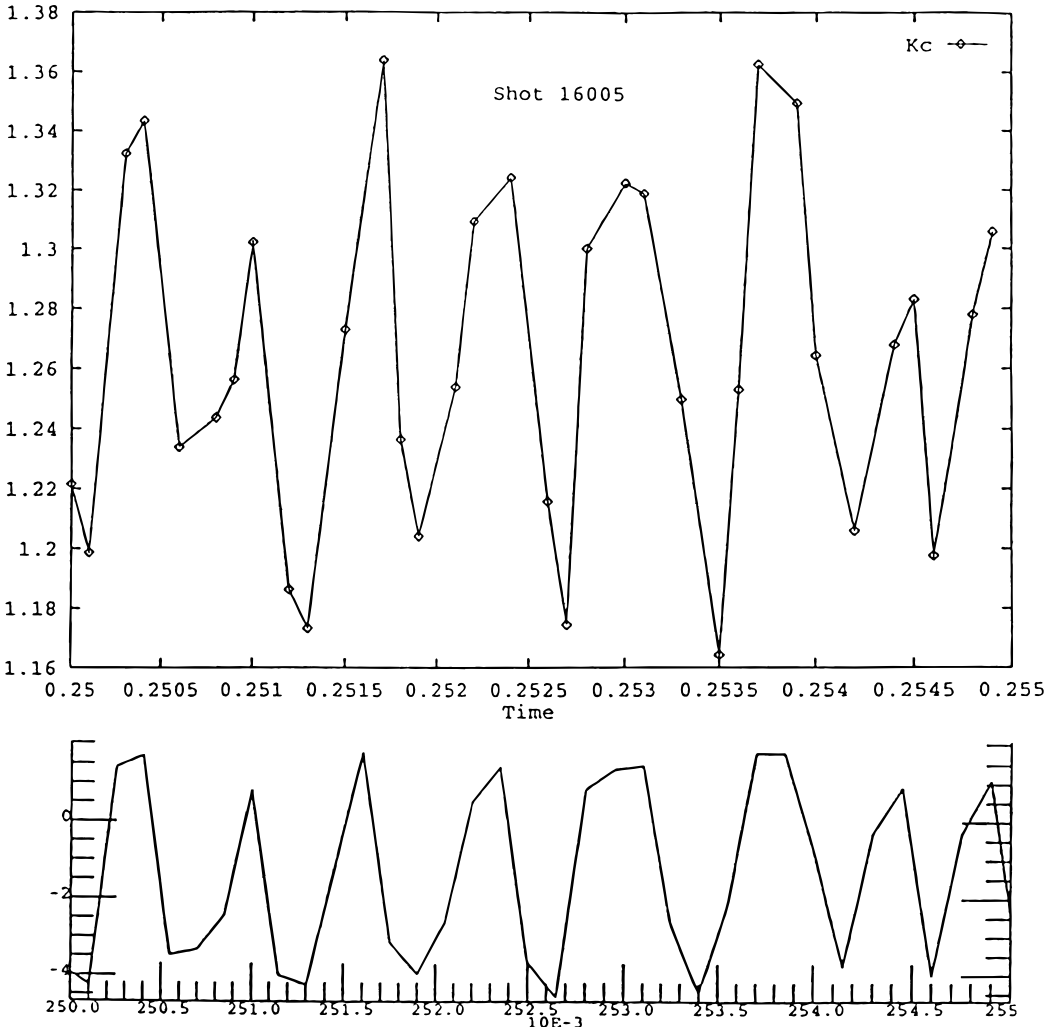

Fig. 10. The core elongation output of the SX neural network over the time interval from 0.25 to 0.255 s.

The inclusion of real experimental data in Sec. V shows all too clearly the difficulties of obtaining diagnostic data to the accuracy needed to make full use of the neural network and other analysis methods. None of the results yet obtained are close to the accuracy required for ITER. The results show the utility of the additional information given by SXs and by CCs. They also demonstrate the feasibility of the neural network method to include several diagnostic techniques.

The real-time SX is now installed on COMPASS-D and is giving its first results. Experience with the magnetic input network now running is that the simulation closely follows the experiment, so the results given here are unlikely to change significantly. The remote FLs are now collecting data on COMPASS-D; however, their analysis must await a new database with a spatially extended computational grid.

ACKNOWLEDGMENT

This work was supported by the U.K. Department of Trade and Industry and Euratom.

REFERENCES

1. D. E. RUMELHART, G. HINTON, and G. WILLIAMS, "Learning Internal Representations by Error Propagation," *Parallel Distributed Processing*, MIT Press, Cambridge, Massachusetts (1986).

2. C. G. WINDSOR, "The Use of Neural Networks in Pattern Recognition and Control," *Syst. Sci.*, **19**, 31 (1993).

3. C. M. BISHOP, *Neural Networks for Pattern Recognition*, Oxford University Press, Oxford, United Kingdom (1995).

4. V. D. SHAFRANOV, "On Magneto-Hydrodynamical Equilibrium Configurations," *Sov. Phys. JETP*, **8**, 710 (1958).

5. C. M. BISHOP, P. COX, P. S. HAYNES, C. M. ROACH, M. E. U. SMITH, T. N. TODD, and D. L. TROTMAN, "Hardware Implementation of a Neural Network to Control Plasma Position in COMPASS-D," *Proc. 17th. Int. Symp. Fusion Technology*, Rome, Italy, September 14–18, 1992, Vol. 2, p. 997, Elsevier.

6. J. B. LISTER and H. SCHNURRENBERGER, "Fast Non-Linear Extraction of Plasma Equilibrium Parameters Using a Neural Network Mapping," *Nucl. Fusion*, **31**, 1291 (1991).

7. J. B. LISTER, H. SCHNURRENBERGER, N. STAEHELI, N. STOCKHAMMER, P.-A. DUPERREX, and J. M. MORET, "Neural Networks in Front-End Processing and Control," IEEE, p. 49 (1992).

8. T. WIJNANDS, "Diagnostics for Long-Pulse Shape and Position Control," ITER Task Report DG1, United Kingdom Atomic Energy Authority (1994).

9. D. A. HUMPHREYS, J. A. LEUER, A. G. KELLMAN, S. W. HANEY, R. H. BULMER, L. D. PEARLSTEIN, and A. PORTONE, "Toward a Design for the ITER Plasma Shape and Stability Control System," *Fusion Technol.*, **26**, 331 (1994).

10. C. G. WINDSOR, P. S. HAYNES, D. L.TROTMAN, M. E. U. SMITH, T. N. TODD, and M. VALOVIC, "On-Line Control of the COMPASS-D Tokamak Using a Neural Network," *Nucl. Energy*, **34**, 85 (1995).

11. L. L. LAO, H. ST. JOHN, R. D. STAMBAUGH, and W. PFEIFFER, "Separation of β_p and l_i in Tokamaks of Non-Circular Cross-Section," *Nucl. Fusion*, **25**, 1421 (1983).

Colin George Windsor (BA, 1960, and DPhil, 1963, University of Oxford, United Kingdom, 1963; Hon. Prof. University of Birmingham, United Kingdom, 1990) has worked on applications of neural networks since 1987. These have included signature and face recognition, stock market index prediction, defect classification from ultrasonics, and gas chromatography elastic matching. Since 1993, he has worked on the reconstruction, control, and disruption prediction of tokamak plasmas.

Thomas Noel Todd (BSc, Imperial College, London University, United Kingdom, 1975) is currently Diagnostics Department manager with United Kingdom Atomic Energy Authority (UKAEA) Fusion with responsibilities for personnel, resource management, and safety. His current interest is the development of ultralow-aspect-ratio tokamaks as a viable option for long-term fusion power. He was one of the original inventors of the START spherical tokamak at Culham and is well known for his activities in toroidal magnetic confinement fusion engineering.

David Leonard Trotman (BA, Open University, United Kingdom, 1982) is manager of the Electronics Group of the Diagnostics Department at UKAEA Fusion. He is responsible for the design and development of the electronics for a large proportion of the plasma diagnostics for COMPASS. He is currently developing systems incorporating fast analogue electronics and is expanding into digital signal processing.

Michael Edward Underhill Smith (BSc, University of Salford, United Kingdom, 1971) is an electronics designer responsible for the design, commissioning, and operations of the analogue and digital electronics used by UKAEA Fusion.